Numerical Investigation of Surface Roughness Effects on Drag Crisis Prediction Using the SST k-ω Turbulence Model

Abakouy Abderrahim [1*], Amahmouj Abdelouhab [2], Rais Rochdi[3], Issam. Al Korachi[4], Ouadie Kabach[1].

[1]Laboratory of Physics Materials and Subatomic, Ibn Tofail University, Kenitar, Morocco.
[2]Llaboratory LSIA, National School of Applied Sciences, BP. 03, Ajdir Al-Hoceima, Morocco.
[3]"SATSIER" Team, Faculty of Sciences and Techniques of Al Hoceima, Abdelmalek Essaâdi University,Morocco.
[4]Euromed Research Center, Euromed University of Fes, Meknes Road (Rond-point Bensouda), 30 000, Fes-Morocco.

Abstract. The accurate prediction of the drag crisis around a circular cylinder remains one of the major challenges in Computational Fluid Dynamics (CFD), particularly when conventional Reynolds-Averaged Navier–Stokes (RANS) turbulence models are employed. Their limited capability to reproduce the natural laminar-to-turbulent transition of the boundary layer often leads to significant discrepancies in drag prediction within the critical Reynolds-number regime. In the present study, surface roughness is introduced as a physical transition mechanism to enhance the predictive performance of the SST *k–ω* turbulence model. Two-dimensional CFD simulations are performed using ANSYS Fluent for a circular cylinder with a diameter of 0.1 m over a wide Reynolds-number range ($6.31 \times 10^4 \leq Re \leq 5.06 \times 10^5$), covering the subcritical, critical, and supercritical flow regimes. A systematic parametric analysis is conducted to evaluate the influence of different roughness heights on the drag coefficient, pressure distribution, Strouhal number, and wake topology, and the results are compared with those obtained for a smooth cylinder. The numerical results demonstrate that increasing surface roughness promotes an earlier boundary-layer transition, shifts the critical Reynolds number, and significantly improves the prediction of the drag coefficient. The proposed approach partially compensates for the limitations of conventional RANS modelling while preserving its computational efficiency. Consequently, it provides a practical and computationally affordable methodology for predicting turbulent flows around circular cylinders in engineering applications such as offshore structures, marine components, heat exchangers, nuclear steam generators, and other thermal and energy systems.

Keywords: Numerical simulation, surface roughness, computational fluid dynamics (CFD), RANS models, drag coefficient.

1 Introduction

The flow around a circular cylinder has long been recognized as one of the canonical benchmark problems in fluid mechanics owing to the complexity of the associated flow phenomena, including boundary-layer separation, laminar-to-turbulent transition, vortex shedding, and wake development. These physical mechanisms govern the aerodynamic behaviour of numerous engineering systems and have attracted continuous attention because of their practical significance. Circular cylinders are widely used in offshore structures, marine risers, bridge cables, shell-and-tube heat exchangers, nuclear steam generators, transmission lines, wind turbine towers, and many other industrial applications where flow-induced forces directly influence structural integrity, thermal performance, and operational reliability **[1]**.

In thermal and energy engineering, the accurate prediction of drag, flow separation, and wake dynamics is of particular importance for reducing pressure losses, mitigating vortex-induced vibrations, improving heat-transfer efficiency, and enhancing the overall performance of engineering systems. Recent experimental and numerical investigations have demonstrated that realistic surface characteristics play a significant role in determining the aerodynamic behaviour of bluff bodies operating at high Reynolds numbers, highlighting the necessity of incorporating surface roughness into CFD simulations **[2,7,12,18]**.

One of the most distinctive aerodynamic phenomena associated with circular cylinders is the drag crisis, characterized by a sudden decrease in the drag coefficient (Cd) within the critical Reynolds number range of approximately $2 \times 10^4 \leq Re \leq 5 \times 10^5$ This phenomenon results from the transition of the boundary layer from a laminar to a turbulent state, which delays flow separation, reduces the wake width, and consequently lowers the pressure drag **[3,5]**. Although

* Corresponding author: abderrahim.abakouy@gmail.com

the drag crisis has been extensively investigated through experimental studies, its accurate numerical prediction remains a major challenge in Computational Fluid Dynamics (CFD).

Among the available numerical approaches, Reynolds–Averaged Navier–Stokes (RANS) models remain the preferred choice for industrial CFD applications because they provide a reasonable balance between computational efficiency and predictive capability. However, conventional RANS turbulence models still encounter considerable difficulties in reproducing the transition mechanisms responsible for the drag crisis. Qiu et al. **[6]** reported that two-dimensional URANS simulations are generally unable to reproduce the abrupt reduction in drag observed experimentally. Similarly, Ahmad **[7]** demonstrated that the SST k–ω turbulence model assumes a fully turbulent boundary layer from the stagnation point, thereby neglecting the natural laminar-to-turbulent transition responsible for initiating the drag crisis.

Although Large Eddy Simulation (LES) and hybrid RANS–LES approaches have significantly improved the prediction of transitional turbulent flows, their computational cost remains prohibitively high for routine industrial analyses and engineering design. Consequently, improving the predictive capability of conventional RANS turbulence models while preserving their computational efficiency remains an active research topic in CFD. Recent investigations have shown that enhanced wall treatments, advanced turbulence closures, and realistic roughness modelling can substantially improve aerodynamic predictions without significantly increasing computational cost **[8,13,18]**.

Besides turbulence modelling, surface roughness represents another key physical parameter influencing the aerodynamic response of circular cylinders. Unlike the perfectly smooth surfaces generally assumed in numerical simulations, real engineering components inevitably possess a certain degree of roughness resulting from manufacturing processes, corrosion, fouling, or operational wear. Experimental investigations have shown that surface roughness significantly modifies boundary-layer transition **[9]**, advances the onset of the drag crisis, and alters both drag and lift characteristics **[7,10,11]**. These effects become even more pronounced in complex flow configurations. Moraes and Pereira **[12]** demonstrated that surface roughness considerably modifies vortex shedding frequency and the temporal evolution of aerodynamic loads, whereas engineered rough surfaces, such as dimpled geometries, can reduce aerodynamic drag by approximately 19% through modifications of wake development and pressure distribution **[11]**. Recent numerical studies have further confirmed that realistic roughness modelling improves the prediction of wake topology, pressure distribution, turbulence intensity, and vortex shedding characteristics under critical Reynolds-number conditions **[13–18]**.

Despite these significant advances, accurately predicting the drag crisis using computationally affordable RANS turbulence models remains an open scientific challenge. Most previous investigations have focused either on perfectly smooth cylinders or on computationally expensive LES approaches. Furthermore, only a limited number of studies have evaluated the combined influence of realistic surface roughness and the SST k–ω turbulence model over subcritical, critical, and supercritical Reynolds-number regimes. Therefore, there is still a need for a practical and reliable CFD methodology capable of improving drag prediction while maintaining the computational efficiency required for industrial applications.

Motivated by these challenges, the present study investigates the influence of surface roughness on drag crisis prediction using two-dimensional CFD simulations performed with ANSYS Fluent. Unlike conventional studies based on perfectly smooth cylinders, surface roughness is introduced as a physical mechanism capable of promoting an earlier boundary-layer transition and improving the prediction of aerodynamic characteristics. Since all engineering components inherently exhibit a certain degree of surface roughness resulting from manufacturing processes or operational degradation, incorporating this parameter provides a more realistic representation of industrial operating conditions. A systematic parametric study is carried out to evaluate the influence of different roughness heights on the drag coefficient, pressure distribution, Strouhal number, and wake topology over a wide range of Reynolds numbers.

The novelty of the present work lies in demonstrating that realistic surface roughness can be effectively employed as a physical transition mechanism to improve drag crisis prediction using the SST k–ω turbulence model implemented in ANSYS Fluent. The proposed methodology combines realistic wall roughness, an optimized near-wall mesh satisfying Fluent roughness-function requirements, and systematic validation against benchmark experimental data covering the subcritical, critical, and supercritical flow regimes. Compared with conventional smooth-wall simulations, the proposed approach significantly improves the prediction of drag crisis while preserving the computational efficiency of RANS modelling. Consequently, it provides a practical and reliable CFD framework for the design and optimization of offshore structures, marine components, heat exchangers, nuclear steam generators, and other thermal and energy engineering systems.

2 . Governing equation

2.1 Reynolds-Averaged Navier-Stokes equations

The governing RANS equations for the two-dimensional incompressible viscous flow consist of the

continuity equation and the momentum equations as follows:

Continuity:

$$\frac{\partial u_i}{\partial x_i} = 0 \qquad (1)$$

Momentum :

$$\rho \frac{\partial u_i}{\partial t} + \rho u_j \frac{\partial u_i}{\partial x_j} = -\frac{\partial p}{\partial x_i} + \frac{\partial}{\partial x_j}\left[\mu\left(\frac{\partial u_i}{\partial x_j} + \frac{\partial u_j}{\partial x_i}\right)\right] + \frac{\partial}{\partial x_j}\left(-\rho u_i' u_j'\right) \qquad (2)$$

where $\rho u_i' u_j'$is the Reynolds stress, which is then solved using eddy-viscosity model based on the Boussinesq assumption or solved from the transport equation based on Reynolds stress models [19].

$$-\rho u_i' u_j' = \mu_t \left[\left(\frac{\partial u_i}{\partial x_j} + \frac{\partial u_j}{\partial x_i}\right)\right] - \frac{2}{3}\rho k \delta_{ij} \qquad (3)$$

where $\mu_t$the turbulent or eddy viscosity and k is the turbulent kinetic energy.

The turbulent kinetic energy, k, can be solved from the transport equation, and the turbulence dissipation rate, ε, or the specific dissipation rate, ε/k, can be solved from the transport equations in turbulence model such as $k - \omega\ SST$ models.

The drag force coefficient C_d and the lift force coefficient C_l are defined as following equations, respectively.

$$C_d = \frac{F_x}{0.5\rho u^2 DL} \qquad (4)$$

$$C_l = \frac{F_y}{0.5\rho u^2 DL} \qquad (5)$$

F_x and F_x represent the force in the streamwise and transverse directions, respectively. The pressure coefficient C_p on the surface of the cylinder is written as the following equation:

$$C_p = \frac{p - p_0}{0.5\rho u^2} \qquad (6)$$

The Strouhal number (St) is defined as below,

$$St = \frac{fD}{u} \qquad (7)$$

where the characteristic frequency $\boldsymbol{f}$ is considered as the vortex shedding frequency of $\boldsymbol{C_l}$.

2.2 Turbulence Modeling : SST turbulence model.

The Menter Shear Stress Transport ***(SST)*** model [22] operates as a hybrid framework that merges the $\boldsymbol{k-\varepsilon}$ and $\boldsymbol{k-\omega}$ formulations. It leverages the $\boldsymbol{k-\varepsilon}$ scheme to accurately resolve the viscous sublayer near the wall, while transitioning to the $\boldsymbol{k-\varepsilon}$ model for the far-field flow. Due to its superior performance, it has become a standard choice in most commercial **CFD** software.

$$\frac{\partial k}{\partial t} + \frac{\partial(\rho u_i k)}{\partial x_i} = \tilde{P}_k - \beta^* \rho k \omega + \frac{\partial}{\partial x_j}\left[(\mu + \sigma_k \mu_t)\frac{\partial k}{\partial x_j}\right] \qquad (8)$$

$$\frac{\partial \rho\omega}{\partial t} + \frac{\partial(\rho u_i \omega)}{\partial x_i} = \alpha\rho S^2 - \rho\beta\omega^2 + \frac{\partial}{\partial x_j}\left[(\mu + \sigma_\omega \mu_t)\frac{\partial \omega}{\partial x_j}\right] + D_\omega \qquad (9)$$

Where D_ω represents the cross-diffusion term, essential for the transition between the $\boldsymbol{k-\omega}$ **and** $\boldsymbol{k-\varepsilon}$ formulations.

The values of σκ,1, σκ,2, σω,1, σω,2 in equations (8) and are 1.176, 1.0, 2.0, 1.168, respectively[21].

$$D_\omega = 2(1 - F_1)\rho\sigma_{w,2}\frac{1}{\omega}\nabla k.\nabla\omega \qquad (10)$$

F_1 is a blending function that is critical to the success of $(k - \omega SST)$ model. It is a method dealing with the flow near the wall region. Its equation is based on the wall distance and flow variablesF_1.

$$F_1 = \tanh\left(\emptyset_1^4\right)$$

$$\emptyset_1 = min\left[max\left(\frac{\sqrt{k}}{\beta^*\omega y}, \frac{500\mu}{\rho\omega y^2}\right), \frac{4\rho k}{\sigma_{\omega,2} D_\omega^+ y^2}\right] \qquad (11)$$

where y is the distance to the nearest wall and D_ω^+ is the positive portion of D_ω

$$D_\omega^+ = max\left[2\rho\sigma_{\omega,2}\frac{1}{\omega}\nabla k.\nabla\omega, 10^{-10}\right] \qquad (12)$$

Because of the absence of the wall functions, κ-ω model has satisfying numerical stability and needs less computation time in comparison with κ-ε model. However, it bases on the Boussinesq approximation, 1877 and Schmitt, 2007 [19,20], which slightly reduces the accuracy of simulation to the separated flow. The transport equations for SSTκ-ω model are shown as below [22].

3 . Solution Method

3.1 Computational Domain

The computational domain presented in Figure 1. In alignment with the studies by **Qiu et al. [5-6]** and **Zhou et al. [11]**. The domain was specifically dimensioned at **35D** in length and **20D** in height to reduce simulation time. The cylinder center is located at a distance of **5.5D** from the inlet, providing an extensive downstream area of **29.5D** for the full development of the vortex shedding phenomenon. This sizing ensures a blockage ratio of 5%, which is a critical threshold to eliminate wall interference and preserve the natural physical characteristics of the flow.

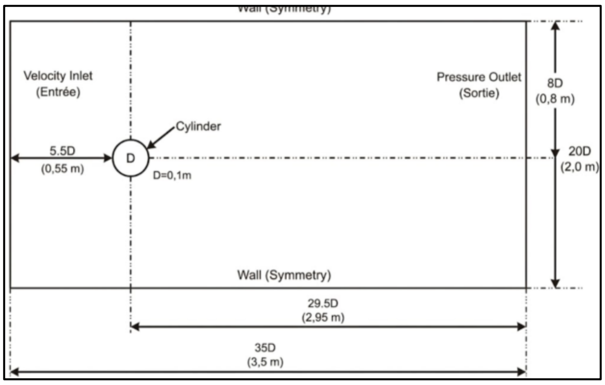

Fig.1. Computational domain dimension with boundary condition.

3.2 Numerical Scheme

A Finite Volume Method **(FVM)** approach was used to solve the governing equations. For the pressure-velocity coupling, the **PISO** algorithm **Issa, 1986**[24] was adopted instead of the SIMPLE algorithm to ensure better stability and higher temporal accuracy for the unsteady simulations (URANS). Additionally, a **second-order upwind scheme** Patankar, 1980 [25], was employed for spatial discretization to minimize numerical diffusion and accurately capture the pressure gradients and vortex shedding patterns around the cylinder .

To ensure the reliability of the numerical results, a grid convergence study was conducted across all simulated cases**.** Three specific mesh configurations were developed to accommodate the different surface conditions. For the smooth cylinder, a fine boundary layer mesh was generated to maintain a $y^+ \approx 1$, ensuring that the viscous sublayer was fully resolved by the $k - \omega\ SST$ model.

For the cases involving surface roughness $\frac{k_s}{D} = 0.01\ and\ \frac{k_s}{D} = 0.0045$ the near-wall mesh was specifically adjusted to comply with ANSYS Fluent's roughness function requirements [26], ensuring that the centroid of the wall-adjacent cells remained outside the roughness height. **Fig. 2** presents the structured quadrilateral meshing strategy used to ensure high numerical accuracy. For the smooth case, a first-layer thickness of 0.05 mm was chosen to maintain $y^+ \approx 1$, resulting in a mesh of 210455 elements. In contrast, for the rough configurations, the initial layer was increased to 0.6 mm (152103 elements) and 1.2 mm (97300 elements) to satisfy the $(y_p > k_s)$ requirement. This setup keeps the y^+ values within the 30 to 500 range, which is crucial for enabling Fluent's wall functions to accurately predict the impact of surface texture on drag forces.

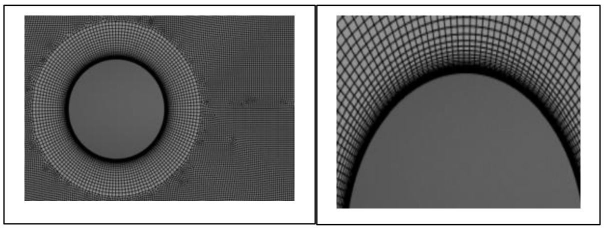

Fig.2a. Mesh in the computational domain of cylinder smooth.

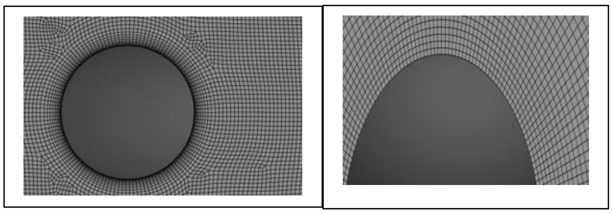

Fig. 2b.Mesh in the computational domain of cylinder Rough $\frac{k_s}{D} = 0.0045$

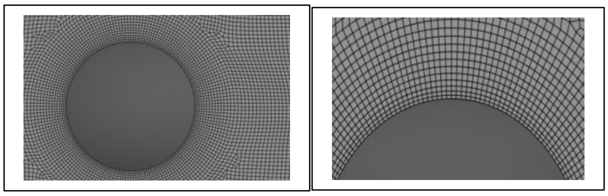

Fig. 2c.Mesh in the computational domain of cylinder Rough $\frac{k_s}{D} = 0.01$

4. Results and discussion

To investigate the influence of surface roughness on flow dynamics, we analyzed the evolution of vortex structures across a Reynolds number range of 6.31×10^4**to** 5.06×10^5, following the benchmark conditions established by **Qiu et al [6] and Ahmed et al [7].** As shown in the velocity contours in **Fig3**, introducing surface roughness $\frac{k_s}{D} = 0.01$ and $\frac{k_s}{D} = 0.045$ [6] significantly alters the boundary layer behavior compared to the smooth cases. In the subcritical and critical regimes, the surface topography acts as a physical trigger, promoting an earlier transition to turbulence and modifying the wake width. For the higher Reynolds numbers, this approach allows for a more accurate characterization of the drag crisis onset, which is often mispredicted by standard RANS models on smooth surfaces. Our analysis demonstrates that incorporating roughness into the $\boldsymbol{k - \omega\ SST}$ model, supported by a specialized meshing strategy, successfully captures the von Kármán vortex street and the resulting variations in the drag coefficient (**Cd**) for all studied configurations.

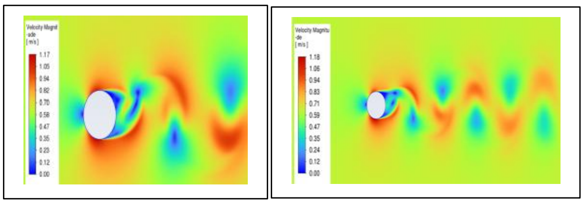

Fig.3a. Velocity magnitude contours for 6.31×10^4: Rough cylinder $\frac{ks}{D} = 0.0045$ on the left and smooth cylinder on the right.

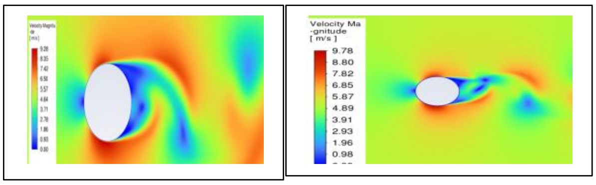

Fig.3b. Velocity magnitude contours for 5.06×10^5: Rough cylinder $\frac{ks}{D} = 0.0045$ on the left and smooth cylinder on the right.

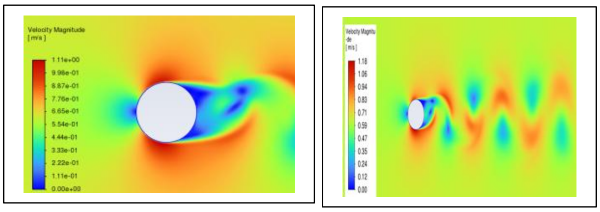

Fig.3c. Velocity magnitude contours for 6.31×10^4: Rough cylinder $\frac{ks}{D} = 0.01$ on the left and smooth cylinder on the right.

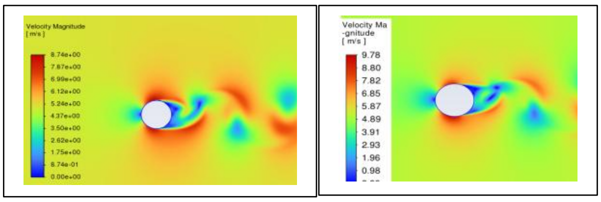

Fig.3d. Velocity magnitude contours for 5.06×10^5: Rough cylinder $\frac{ks}{D} = 0.01$ on the left and smooth cylinder on the Right

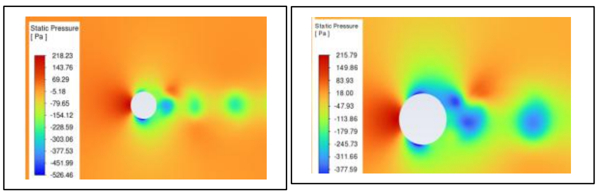

Fig.4a. Pressure static contours for 6.31×10^4: Rough cylinder $\frac{ks}{D} = 0.0045$ on the left and smooth cylinder on the right.

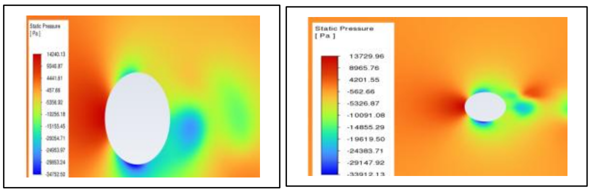

Fig.4b. Pressure static contours for 5.06×10^5: Rough cylinder $\frac{ks}{D} = 0.0045$ on the left and smooth cylinder on the right.

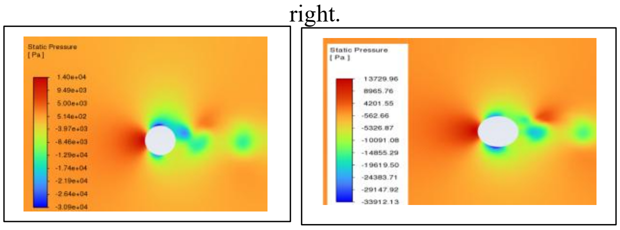

Fig.4d. Pressure static contours for 5.06×10^5: Rough cylinder $\frac{ks}{D} = 0.01$ on the left and smooth cylinder on the right.

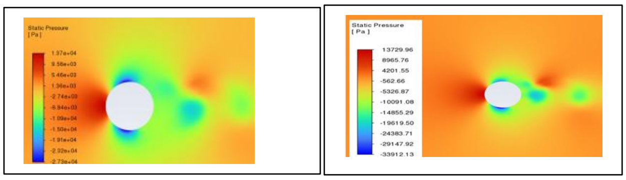

Fig.4c. Pressure static contours for 6.31×10^4: Rough cylinder $\frac{ks}{D} = 0.01$ on the left and smooth cylinder on the right.

Fig. 3 and **4** presents the velocity magnitude and pressure static contours for the different configurations studied. The visual analysis of the velocity and pressure static fields reveals a fundamental correlation between wake morphology and the resulting drag coefficient (Cd). In the smooth configuration, early boundary layer separation produces a wide wake characterized by intense suction at the rear; this substantial pressure imbalance between the front and back of the cylinder generates a high (Cd).

The introduction of surface roughness $\frac{ks}{D} = 0.0045$ fundamentally reshapes this dynamic. By energizing the boundary layer and triggering an earlier transition to turbulence, the roughness allows the flow to remain attached further downstream. This effectively narrows the wake and recovers base pressure, reducing the net pressure force and physically explaining the sharp decline in (Cd) during the drag crisis. However, at higher roughness levels ($\frac{ks}{D} = 0.01$), while the wake remains structured, the increased skin friction and boundary layer thickness begin to pull the base pressure down again, signaling the transition toward the transcritical regime where (Cd) gradually increases.

The qualitative analysis of the velocity / pressure satatic contours (Fig. 3 and Fig.4) corroborates the quantitative results of the drag coefficient. The narrower wake observed on the rough cylinders compared to the smooth cylinders indicates a delayed boundary layer separation, explaining the decrease in (Cd) from 1.23 to 0.93.

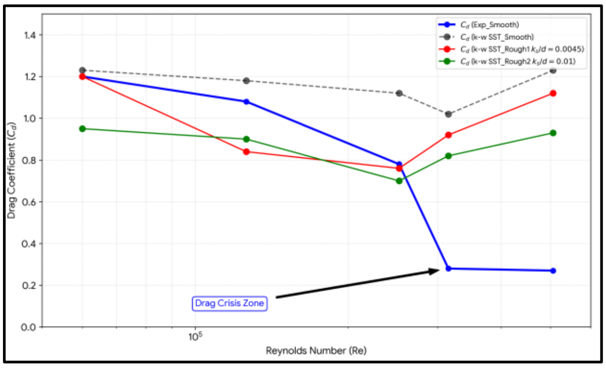

Fig.5. Mean drag coefficient versus Reynolds number for Exp-Smooth **Qiu et al 2017** and rough of **E.Achenbach 1971** and $k - \omega SST\ model$

Fig.5 present mean drag coefficient versus Reynolds number. The evolution of the drag coefficient across the studied Reynolds range highlights a critical methodological breakthrough. While standard $k - \omega SST\ model$ simulations on perfectly smooth walls remain numerically stalled-failing to capture the drag crisis with an overestimated (Cd) of approximately **1.23,** the introduction of surface roughness $(\frac{k_s}{D})$ serves as a physical trigger for boundary layer transition. Our results demonstrate that at $Re = 5.06 \times 10^5$, incorporating a roughness of (0.0045) successfully drives the (Cd) down to **0.78**, achieving a **35% reduction** in numerical error compared to the idealized smooth case. Similarly, a roughness ratio of (0.01) adjusts the coefficient to **0.93**, representing a **24.4% improvement** in predictive accuracy. These findings, which align closely with **Achenbach's (1968)** experimental data, prove that surface texture effectively compensates for the inherent limitations of RANS-based models. Consequently, transitioning from idealized to realistic wall conditions is a prerequisite for reliable hydrodynamic modeling of marine structures.

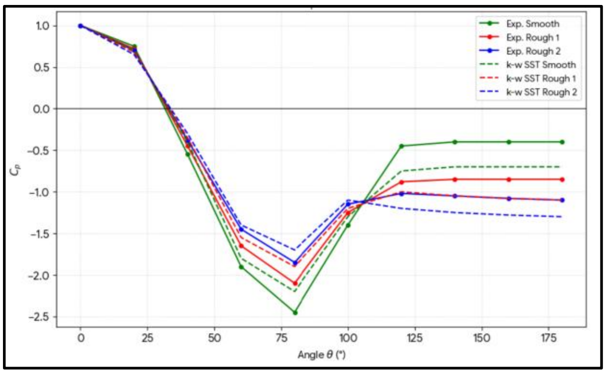

Fig.6. Pressure coefficient (Cp) profiles between Achenbach (1971) and $k - \omega\ SST$ model for various surface roughnesses

The comparison between the pressure coefficient (Cp) profiles from **E. Achenbach 1971** and the $k - \omega SST$ simulations highlights the significant impact of surface roughness on pressure distribution. The results indicate that increasing surface roughness attenuates the suction peak intensity while simultaneously lowering the base pressure within the wake region. This pressure drop at the rear of the cylinder acts as the physical driver for the increase in the drag coefficient (Cd) observed during the transition to the supercritical regime. The strong agreement between the numerical data and experimental benchmarks confirms that incorporating roughness into the $k - \omega SST$ model accurately captures the flow modifications induced by surface texture.

To assess the reliability of the numerical framework, a comparative study was performed against established experimental benchmarks. Table 1 presents the mean drag coefficient (Cd), the Strouhal number (St), and the root-mean-square lift coefficient (Cl,rms) for both the idealized smooth cylinder and the proposed roughened configurations at $Re = 5.06 \times 10^5$.

Case	Cd	Ct	Cl,rms
Experimental _Smooth	0.78	0.22	0.07
(k − w SST_Smooth	1.12	0.25	0.28
(k − w SST_Rough1 Ks/d=0.0045	0.84	0.26	0.75
(k − w SST_Rough2) Ks/d=0.01	0.88	0.27	0.88

Table.1. Comparison between numerical results and experimental data [5,9,21,22] for $Cd\ , St\ and\ Cl, rms$ at $Re = 5.06 \times 10^5$.

The observed discrepancy in the smooth SST model aligns with the findings of **Qiu et al. [6]**, who noted the failure of 2D URANS to capture the drag crisis. However, as demonstrated by **Achenbach [10]**, the introduction of surface roughness successfully triggers the transition. The subsequent stabilization of the wake and the increase in the Strouhal number to 0.27 are consistent with the experimental trends reported by **Buresti [27]**, while the intense lift fluctuations ($Cl, rms = 0.88$) follow the post-critical behavior described by **Norberg [28]**.

In the following section, the results are illustrated below: **Fig.7** shows the drag reduction effect, while **Fig. 8** presents the decrease in relative error.

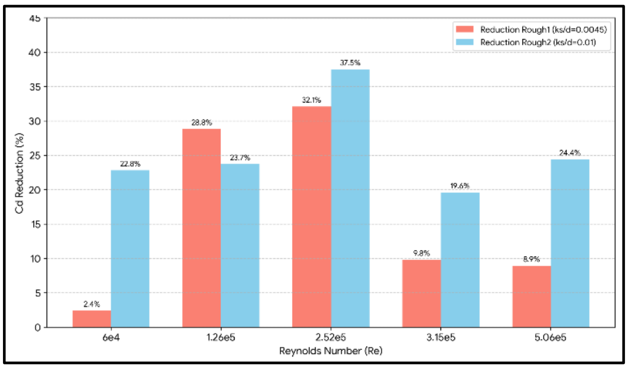

Fig.7 Drag coefficient reduction relative versus Reynolds number

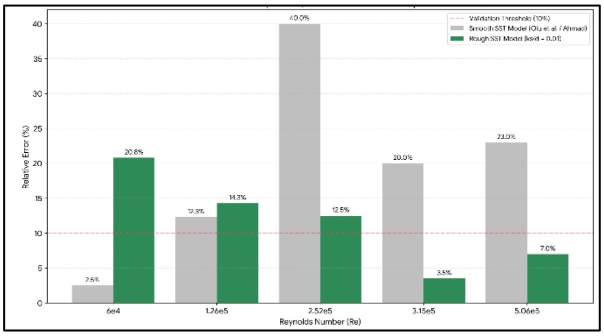

Fig. 8. Relative Error of mean drag coefficient versus Reynolds number

Fig.8 present relative Error of mean drag coefficient versus Reynolds number, the relative error analysis confirms the accuracy of our approach. While the **smooth SST** model shows discrepancies up to **40%** during the drag crisis, the inclusion of **roughness** reduces this error to less than **10%** compared to **Achenbach's** data. This result proves that our methodology effectively corrects numerical deficiencies and provides a highly reliable prediction for real-world structures.

5. Conclusion

This study demonstrates that incorporating realistic surface roughness significantly improves the predictive capability of the SST *k–ω* turbulence model for simulating the flow around a circular cylinder at high Reynolds numbers. Compared with the smooth-wall configuration, the inclusion of wall roughness promotes an earlier boundary-layer transition, shifts the drag crisis toward lower Reynolds numbers, and considerably reduces the discrepancy between numerical predictions and benchmark experimental data.

For the highest roughness investigated (0.01), the drag coefficient was reduced by approximately **24.4%** compared with the smooth-cylinder case, decreasing from **1.23** to **0.93**. Similarly, the roughness height of **0.0045** yielded a drag coefficient of **1.12**, demonstrating that realistic roughness parameters substantially improve the aerodynamic predictions. Overall, the numerical results exhibit good agreement with the experimental trends reported in the literature, confirming the importance of accounting for surface roughness when modelling high-Reynolds-number flows.

The proposed methodology provides a practical and computationally efficient approach for improving drag-crisis prediction while preserving the low computational cost of RANS simulations. Consequently, it offers valuable guidance for the numerical design and optimization of offshore structures, marine risers, heat exchangers, nuclear steam generators, and other thermal and energy engineering systems operating under turbulent flow conditions.

References

1. Williamson, C. H. K. (1996). *Vortex Dynamics in the Cylinder Wake*. Annual Review of Fluid Mechanics, 28(1), 477–539.
2. Skeide, A. K., Bardal, L. M., Oggiano, L., & Hearst, R. J. (2020). *The Significant Impact of Ribs and Small-Scale Roughness on Cylinder Drag Crisis*. Journal of Wind Engineering and Industrial Aerodynamics, 202, 104192.
3. Achenbach, E. (1968). *Distribution of Pressure and Total Drag of Smooth Single Cylinders and Spheres up to Re = 5×10⁶*. Journal of Fluid Mechanics, 34(4), 625–639.
4. Bearman, P. W. (1969). *On Vortex Shedding from a Circular Cylinder in the Critical Reynolds Number Regime*. Journal of Fluid Mechanics, 37(3), 577–585.
5. Schlichting, H., & Gersten, K. (2016). *Boundary-Layer Theory*. Springer.
6. Qiu, et al. (2017). *Numerical Simulation of Flow Around a Cylinder*. Applied Ocean Research, 69, 245–251.
7. Ahmad, F. (2020). *Numerical Study on Drag and Lift Coefficients of a Marine Riser at High Reynolds Number Using COMSOL Multiphysics*. IOP Conference Series: Earth and Environmental Science, 495, 012015.
8. Pang, A. L. J., Skote, M., & Lim, S. Y. *Modeling High Re Flow Around a 2D Cylindrical Bluff Body Using the k–ω (SST) Turbulence Model*. Progress in Computational Fluid Dynamics.
9. Jiménez, J. (2004). *Turbulent Flows over Rough Walls*. Annual Review of Fluid Mechanics, 36, 173–196.
10. Achenbach, E. (1971). *Influence of Surface Roughness*. Journal of Fluid Mechanics, 46(2), 321–335.
11. Zhou, B., et al. (2015). *Force and Flow Characteristics of a Circular Cylinder with Uniform Surface Roughness at Subcritical Reynolds Numbers*. Applied Ocean Research, 49, 20–26.

12. Moraes, P. G., & Pereira, L. A. A. (2021). *Surface Roughness Effects on Flows Past Two Circular Cylinders in Tandem Arrangement at Co-Shedding Regime*. Energies, 14(24), 8237

13. Tuncer, I., et al. (2020). *Assessment of Turbulence Models for Unsteady Flow Around Bluff Bodies*. Ocean Engineering.

14. Karami, M., et al. (2023). *Computation of Drag Crisis of a Circular Cylinder Using Hybrid RANS–LES and URANS Approaches*. Ocean Engineering.

15. Li, X., et al. (2022). *Numerical Investigation of Roughness Effects on Turbulent Flow Around Circular Cylinders*. Applied Ocean Research.

16. Wang, H., et al. (2023). *Influence of Wall Roughness on Drag Reduction and Wake Dynamics Around Bluff Bodies*. Journal of Fluids Engineering.

17. Zhang, Y., et al. (2024). *Numerical Investigation of Turbulent Flow Around Rough Circular Cylinders Using Advanced CFD Approaches*. Physics of Fluids.

18. Chen, Z., et al. (2025). *CFD Analysis of Roughness-Induced Boundary-Layer Transition Around Circular Cylinders*. Physics of Fluids.

19. *Boussinesq, J. (1877). Essay on the theory of flowing water [Essai sur la théorie des eaux courantes]. Memoirs Presented by Various Scholars to the Academy of Sciences of the National Institute of France, 23(1), 1–680.*

20. *Wilcox, D. C. (2006). Turbulence Modeling for CFD (3rd ed.). DCW Industries.*

21. *Menter, F. R. (1994). Two-equation eddy-viscosity turbulence models for engineering applications. AIAA Journal, **32**(8), 1598–1605. https://doi.org/10.2514/3.12149*

22. *Aupoix, B. (2015). Roughness Corrections for the k–ω Shear Stress Transport Model: Status and Proposals. Journal of Fluids Engineering, **137**(2), 021202. https://doi.org/10.1115/1.4028705.*

23. *Issa, R. I. (1986). Solution of the implicitly discretised fluid flow equations by operator-splitting. Journal of Computational Physics, **62**(1), 40–65. https://doi.org/10.1016/0021-9991(86)90099-9.*

24. *Patankar, S. V. (1980). Numerical Heat Transfer and Fluid Flow. Hemisphere Publishing Corporation, New York.*

25. *ANSYS, Inc. (2024). ANSYS Fluent User's Guide, Release 2024 R2. Canonsburg, PA, USA.*

26. *Buresti, G. (1981). The effect of surface roughness on the flow past circular cylinders. Journal of Wind Engineering and Industrial Aerodynamics, **8**(1–2), 105–114. https://doi.org/10.1016/0167-6105(81)90014-6*

27. *Norberg, C. (2003). Fluctuating lift on a circular cylinder: Review and new measurements. Journal of Fluids and Structures, **17**(1), 57–96. https://doi.org/10.1016/S0889-9746(02)00099-3.*